Tracing locations of new coating material during spark anodizing of titanium

Endzhe Matykina, Frederic Louis Monfort, Ahmed Berkani, Peter Skeldon, George Thompson, Patrick Chapon

Tracing locations of new coating material during spark anodizing of titanium

Journal:	*Philosophical Magazine & Philosophical Magazine Letters*
Manuscript ID:	TPHM-05-Jun-0281.R1
Journal Selection:	Philosophical Magazine
Date Submitted by the Author:	21-Jul-2005
Complete List of Authors:	Matykina, Endzhe; The University of Manchester Monfort, Frederic; The University of Manchester Berkani, Ahmed; The University of Manchester Skeldon, Peter; The University of Manchester, Corrosion and Protection Centre Thompson, George; The University of Manchester Chapon, Patrick; Horiba Jobin Yvon
Keywords:	titanium, oxidation, electrochemical
Keywords (user supplied):	anodizing, anodic oxidation

Tracing locations of new coating material during spark anodizing of titanium

E. MATYKINA,[1] F. MONFORT,[1] A. BERKANI,[1] P. SKELDON,[1*] G.E. THOMPSON[1] and P. CHAPON[2]

[1]Corrosion and Protection Centre, School of Materials, The University of Manchester, Sackville Street, P.O. Box 88, Manchester, M60 1QD, United Kingdom

[2]Horiba Jobin Yvon, 16-18 rue de canal, 91165 Longjumeau Cedex, France

The growth of anodic coatings on titanium, under sparking conditions, is investigated in tracer experiments, using alkaline silicate and phosphate electrolytes. Coatings are formed sequentially in each electrolyte, with phosphorus and silicon located by energy-dispersive X-ray analysis and glow discharge optical emission spectroscopy. The coatings, containing anatase, rutile and amorphous oxide, with incorporated phosphorus and silicon species, are shown to grow by discrete thickening at sites of dielectric breakdown. New material is found near the metal, within the coating bulk and at the coating surface. Approximately 10 – 30% of the new material is located near to the coating surface and about 40 – 60% near to the metal. The findings are attributed to the formation of breakdown channels allowing access of electrolyte species to the inner parts of the coating and to subsequent rapid formation of coating material, under high temperatures, associated with increased local current density, and high pressures, associated with volume constraints on oxide growth and gas generation.

Keywords: Anodizing, titanium, dielectric breakdown

1. Introduction

There is an extensive literature on anodizing of aluminium, magnesium and titanium at high potentials, with sparks, or arc micro-discharges, on the anode that assist the development of thick coatings. Such anodizing has been variously called plasma electrolytic oxidation (PEO) [1], anodic oxidation under spark discharge (ANOF) [2,

3], anodic spark deposition (ASD) [4, 5], microplasma electrochemical formation [6] and micro-arc oxidation (MAO). The coatings, typically of the order 10 μm thick, are often ceramic-like, with crystalline and amorphous phases derived from constituents of the metal and of the electrolyte [7, 8]. They have potential applications in which improved surface performance, such as increased hardness and corrosion resistance, is required. Accordingly, a relatively extensive knowledge of the physical and functional properties of coatings is available, as well as of influences of forming conditions. In particular, by control of process conditions, coating properties can be tailored for practical applications [9]. In contrast, the mechanistic understanding of coating growth is less established, largely due to experimental difficulty of probing processes at individual discharge channels, occurring over dimensions of a few microns with durations of < 1 s.

The coating growth has been associated with (i) anodizing of the substrate, (ii) diffusion deposition, (iii) electrophoretic deposition, and (iv) thermal ionization and condensation [1]. High temperatures, 10^3–10^4 K, and pressures, 10^2–10^3 MPa, inside discharge channels support incorporation of electrolyte ions into the coating and assist plasma thermochemical reactions and deposition of melt-quenched oxides and other compounds. In the micro-plasma formation model [10], the discharge channels are heated by electron avalanches. Anions of the electrolyte and melted substrate elements are drawn into the channels, under a high electric field, ~10^6 V/m, with plasma chemical reactions proceeding in association with separation of oppositely charged ions and ejection of cations to the electrolyte. Finally, the channels cool and reaction products are deposited onto their walls.

A scheme of the micro-arc processes under alternating current has been developed [11] involving: (i) aspects of conventional anodizing, including oxide formation due to ionic current flow via discharge channels and anodizing of discharge-free surfaces; (ii) secondary electrochemical processes of gas liberation, such as hydrogen and oxygen, formation of hydrogen peroxide in the electrolyte, and anodic dissolution of the metal; (iii) electrothermally-induced metallurgical processes in the surface layer, which result in local melting, quenching and recrystallisation of surface deposits; (iv) plasma thermochemical reactions, initiated by the current passing via the discharges, involving electrons, molecules of water, electrolyte anions and atoms and ions of the metal, that lead eventually to the deposition of insoluble products [9, 12].

In other work, on coating formation in colloidal electrolytes [8], the proposed mechanism involved thermolysis of hydrated Me(II) or Me(III) polyphosphates that are precipitated at the discharge region, with insoluble products remaining in the coating. For non-colloidal solutions, the coating grows mainly due to electrochemical oxidation of the substrate metal. The role of the breakdown is to intensify mass transfer processes, to produce high-temperature phases, and to create conditions for significant incorporation of electrolyte anions and Me species into the coating. The high coating thickness from colloidal electrolytes was attributed to increased precipitatation on the anode.

A double-layered coating was suggested for coating growth in vanadium and tungsten containing heteropolyoxoanion (HAP) electrolyte [13], with an anodic oxide layer forming in the pre-sparking range. Sparking results in deposition of dissolved salts of HAPs at the anode. Thermolysis proceeds around the breakdown channels, with

insoluble products developing into an outer coating layer. In other studies of aluminium and titanium alloys [14], using cobalt-containing polyphosphate electrolyte, the coating thickened uniformly up to a charge of 2 kC dm^{-2}, while subsequent growth occurred as nodules. Microplasma discharges developed between nodules, ejecting substrate metal ions, which formed a film of approximately constant composition.

Recently, the present authors employed sequential anodizing in the sparking region to introduce tracer species into a coating formed on aluminium [15]. The use of sequential anodizing appears to be a relatively new approach to understanding coating growth under sparking conditions. The coating was formed in silicate electrolyte and then in phosphate electrolyte. Much of the phosphorus incorporated into the coating in the second stage of anodizing was located next to the metal, clearly demonstrating that a significant portion of the coating is created at, or close to, the metal/coating interface. Here, the tracer approach is developed further, on this occasion using titanium, with relatively brief formation of coating in the second stage of anodizing in order to identify more readily the coating growth associated with individual sparks. The main interest is in identifying locations of newly formed material through the coating thickness. The distributions of silicon and phosphorus species are determined by a combination of glow discharge optical emission spectroscopy (GDOES), which provides information over a wide area of surface, and energy-dispersive X-ray (EDX) analysis, which provides information at local regions.

2. Experimental

2.1 Material

Specimens of thermally-annealed, 0.25 mm and 0.05 mm thick, titanium foil (3000 ppm Fe, 750 ppm O, 55 ppm N, <800 ppm C), of typical working area 3 cm^2, were degreased in acetone and ethanol, rinsed in deionized water and polished in a mixture of 48% HF and 70% HNO_3 (1:3 by vol.) for 60 s at room temperature. They were then rinsed with deionized water and dried in warm air.

2.2 Anodizing

Specimens were anodized galvanostatically at 2 A/dm^2, using a regulated DC power supply, in either a single electrolyte or two different electrolytes. The electrolytes, consisting of either 0.05 M $Na_2SiO_3 \cdot 5H_2O$/0.1 M KOH, with pH 12.0 and conductivity 24.3 mS, or 0.026 M Na_3PO_4, with pH 12.0 and conductivity 7.95 mS, were prepared from deionized water and high-purity chemicals. Anodizing was carried out for selected times in the range 600 - 1500 s, with electrolyte stirring, using a double-walled glass beaker, containing a stainless steel cathode. The temperature was controlled at 293 K by an external thermostat. Voltage-time and current-time responses were recorded electronically during anodizing, with a sampling time of 20 ms. After coating, specimens were rinsed with deionized water and dried in warm air.

2.3 Specimen examination

Plan and cross-section views of coated specimens were examined by scanning electron microscopy (SEM), using an Amray 1810 instrument, equipped with EDX analysis facilities. EDX analyses were carried out at two accelerating voltages, 10 and 20 kV, to access different depths of the coating material. Cross-sections were ground through successive grades of SiC paper, followed by finishing to 1 μm diamond. Thickness measurements were also made for each coating using an eddy current meter, with the average of ten measurements cited. Phase structure was investigated by X-ray diffraction (XRD), using a Philips X'Pert – MPD (PW 3040) instrument with a step size 0.005° and a scan range from 5 to 85° (in 2θ). Ultramicrotomed sections, nominally 20 nm thick, of anodized specimens were examined by transmission electron microscopy (TEM), employing a JEOL 2000 FX II instrument. Depth profiling analysis of coatings was carried out by glow GDOES, using a Jobin Yvon 5000 RF instrument, in an argon plasma of 630 Pa, with RF of 13.56 MHz and power of 35 W. Light emissions were monitored, with a sampling time of 0.01 s, at wavelengths of 130.156, 178.221, 288.158, 365.350 and 589.592 nm for oxygen, phosphorus, silicon, titanium and sodium respectively. The signals were detected from a circular area of approximately 4 mm diameter.

3. Results

3.1 Formation of coatings in individual silicate and phosphate electrolytes

The voltage-time behaviour for anodizing titanium in silicate electrolyte revealed an approximately linear region to 100 V, with a slope of about 5 V s^{-1}, followed by a

region of decreasing slope (Figure 1(a)). Visible sparking commenced at about 222 V, with a pronounced inflection on the voltage-time curve evident shortly afterwards. Fluctuations in the current record as early as 100 V suggested preceding film breakdown without sparking. Such fluctuations follow sudden changes in coating resistance due to the breakdown events. Gas evolution was observed soon after the start of anodizing and persisted thereafter, with significant increase following onset of sparking. A broadly similar voltage-time response was found for anodizing in phosphate electrolyte, with sparking being observed from about 290 V (Figure 1(a)). Both coatings were of uniform matt grey appearance, the coating from phosphate electrolyte being slightly lighter. The difference in sparking voltages in the two electrolytes can be attributed to the specific influences of the electrolyte constituents, and the increased resistivity of the phosphate electrolyte.

(Insert Fig 1 near here)

The coatings revealed a decreasing rate of thickening with progress of anodizing in both phosphate and silicate electrolytes (Figure 2). The efficiency of coating growth, estimated from the coating thickness and the charge passed during anodizing, with the assumption of formation of anatase, decreased with progress of anodizing, with average efficiencies in both electrolytes of about 20 % for the thickest coatings investigated, about 8 μm (Table 1).

(Insert Table 1, Fig 2 near here)

The surfaces of coatings developed in the sparking regions of both electrolytes revealed usual pores, typically in the micron size range, associated with breakdown sites (Figure 3). Nodular and raised ring-like features were conspicuous around pores of the coatings formed in silicate electrolyte, but not for the coatings produced in the phosphate electrolyte, which also exhibited some elongated pores.

(Insert Fig 3 near here)

GDOES profiles for the coating formed in phosphate electrolyte revealed oxygen, phosphorus and titanium in most regions of the coating at the available depth and lateral resolutions (Figure 4(a)). Similarly, oxygen, silicon and titanium were distributed throughout the thickness of coatings formed in silicate electrolyte (Figure 4(b)). Both coatings also contained sodium species, which appeared to be present in most regions of the coating, with an increased amount near to the metal. Potassium, which was not determined in the present analyses, is probably distributed similarly to sodium. The time to reach the metal/coating interface, estimated from the half-height of the back edge of the oxygen signal, was about 96 s, compared with about 68 s for the coating formed in silicate electrolyte, due to differences in sputtering rates and coating thicknesses (Figure 2, Table 1). For these and for later specimens, the oxygen signal increased near to the coating surface, while the titanium signal decreased, which may be related to the presence of either increased amounts of silicon and phosphorus species or surface contamination by hydrocarbons.

(Insert Fig 4 near here)

X-ray diffraction indicated coatings formed in silicate and phosphate electrolytes comprised about 35 and 94 % crystalline phases, consisting of anatase and rutile, with the remainder being amorphous material (Figure 5). Anatase was the main phase in the coating formed in phosphate electrolyte, with a shorter anodizing time, 900 s, than that of the coating formed in silicate electrolyte, 1200 s, which contained relatively more rutile.

(Insert Fig 5 near here)

3.2 Sequential anodizing, firstly in silicate and secondly in phosphate electrolytes

The voltage-time response for anodizing titanium for 1500 s to 435 V in phosphate electrolyte, following previous anodizing for 1200 s to 360 V in silicate electrolyte, revealed (i) a surge to about 80 V; (ii) a relatively slow increase to 300 V over 1200 s (iii) a relatively fast rise beyond 300 V, with sparking resuming at 400 V, and (iv) a slow rise to the termination of anodizing (Figure 1(b), Table 2). Gas evolution was evident soon after the commencement of re-anodizing. The average thickness of the coating formed in silicate electrolyte was about 4.3 μm, with about 1.3 μm added in phosphate electrolyte (Table 2), this thickness increase being measured at the thickest parts of the coating. The coating surface revealed uniformly distributed fine regions of light and dark grey material, the former being attributable to the sparking in phosphate electrolyte.

(Insert Table 2 near here)

Scanning electron micrographs of the coating surface disclosed two distinct regions of breakdown morphologies characteristic of the individual silicate and phosphate electrolytes, i.e. nodular features formed in silicate electrolyte and a flatter surface formed in phosphate electrolyte (Figure 6(a)). Evidently, the re-anodizing period in phosphate electrolyte was too short to produce a uniform surface characteristic of the phosphate electrolyte. In accordance with the morphological evidence, EDX analysis confirmed the presence of silicon, but little or no phosphorus, in the nodular region, while phosphorus and a reduced amount of silicon were detected in the relatively flat region (Figures 6(a) and 7, Table 3, in which the point analyses at phosphorus-rich and silicon-rich regions are labeled P and Si, followed by a number, respectively). Thus, about 22 at.% silicon, and less than about 0.3 at.% phosphorus, were identified at the nodular regions, compared with respective values of 0.6 at.% silicon and 7.6 at.% phosphorus at flat regions, with no major influence of the accelerating voltage. Titanium and oxygen were also identified at both regions, in amounts consistent with the presence of titanium oxide, and other oxygen-containing species, although the accuracy of the analyses was not sufficiently high to provide stoichiometric relationships. The analysis over the whole of the imaged area indicated reduced concentrations of phosphorus and silicon, 4.5 and 6.7 at.% respectively, compared with the phosphorus- and silicon-rich regions respectively, as expected (Figure 7, Table 3). At the edge of the phosphorus-containing material, silicon-rich nodules stand proud, indicating a low thickening of the coating by growth at the coating/electrolyte interface (Figure 6(b)). The distribution of surface breaking pores, with dark appearance, suggests that the regions of breakdown in phosphate electrolyte are made up of surface elements comprising a central pore and surrounding flat material extending to about 10 μm.

(Insert Table 3, Figs 6 and 7 near here)

GDOES depth profiles revealed phosphorus and silicon species at the coating surface and throughout most of the coating depth, along with the expected oxygen and titanium species (Figure 4(c)). The phosphorus signal, which is magnified to ease observation, falls steeply during the initial 7 s of sputtering, i.e. in about 10 % of the time for sputtering to the average thickness of the coating, indicative of a comparatively thin phosphorus-enriched outer layer, consistent with SEM. The phosphorus signal also rises near the metal/coating interface, with the peak intensity lying below the depth of the average location of the interface, suggesting locally thicker phosphorus-containing material. The ratio of the silicon and oxygen signals in the coating formed sequentially was reduced compared with that for the coating formed in the individual silicate electrolyte. The time to sputter through the coating formed sequentially, about 72 s, was similar to that for the coating formed in silicate electrolyte. Sodium was distributed throughout the coating, with a significant increase near the metal. The sodium signal near the metal appeared to comprise two peaks, the inner peak correlating with the location of the phosphorus peak. XRD indicated the presence of anatase and rutile in the coating, with about 65% amorphous material (Figure 5).

EDX analyses of a cross-section prepared by ultramicrotomy disclosed regions of the coating where, in addition to titanium and oxygen, mainly silicon was present throughout the coating thickness, with increased levels of silicon in nodules (Figures 6(c) and 7, Table 3). Thus, analysis of a nodule revealed 11 at.% silicon, while about 10 at.% silicon was detected in underlying material. Phosphorus levels were usually

below 0.4 at.%, although an increased value was indicated at the nodule at an accelerating voltage of 10 kV. In adjacent parts of the coating, where the thickness increased locally, mainly phosphorus was detected, at levels of about 5 at.%, including near to the metal, while silicon was a comparatively negligible constituent, below about 0.3 at.%. The dependence of analyses on accelerating voltage, is probably due to roughness, the possible presence of cavities, and non-uniformity of coating composition with depth. Notably, cavities of size up to several microns were evident particularly in the inner part of the coating, with some cavities connecting to the pores at the coating surface. At a region located between two adjacent, phosphorus-rich sites, associated with breakdown in phosphate electrolyte, both phosphorus and silicon were detected at levels of about 2.0 and 6.6 at.% respectively (Figure 7, Table 3).

EDX analyses were also carried out at residues of the coating material observed in scanning electron micrographs of the bottom of the sputtering crater created during GDOES profiling, disclosing phosphorus, but not silicon, species (Figure 8, Table 3). The apparent phosphorus concentration was 2.8 at.%, although the electron beam penetrated to the underlying metal, as evident by the enhanced signal from titanium. The pattern of regions containing residual coating material was similar to that of the breakdown tracks formed in the phosphate electrolyte at the coating surface. The finding indicates that the location of the interfacial phosphorus peak in the GDOES profile is due to locally deeper regions of phosphorus-containing coating material.

(Insert Fig 8 bear here)

Transmission electron micrographs of the coating revealed amorphous and crystalline material, located both next to the metal and at more remote regions (Figure 9). The sectioning resulted in mechanical damage to the coating, which limited observations mainly to the inner material of the coating layer.

(Insert Fig 9 near here)

3.3 Sequential anodizing, firstly in phosphate and secondly in silicate electrolytes

Sequential anodizing of titanium for 900 s to 435 V in phosphate electrolyte and then for 600 s to 380 V in silicate electrolyte resulted in fast recovery of breakdown compared with the opposite sequence of electrolytes, with visible sparking commencing at 380 V, accompanied by gas evolution, and a final period of very slow voltage rise (Figure 1(c), Table 2). The difference in pre-sparking voltage-time responses for the second stages of the two re-anodizing experiments, not being of direct relevance to the present interests, will be considered elsewhere. The coating was of uniform grey appearance, similar to the coating formed in silicate electrolyte. The thickness of the coating increased from 5.1 to 6.7 μm following the two stages (Table 2). The total time of sparking in the second electrolyte was about 50% longer than that in the previous experiment.

The surface of the coating contained raised features around pores, reminiscent of breakdown in silicate electrolyte, although nodules were absent, possibly associated with the increased final voltage and influence of pre-existing phosphorus-containing material (Figure 10). There was no obvious coating material characteristic of a surface

formed in phosphate electrolyte. EDX analysis of the imaged area revealed about 2.3 at.% phosphorus and 5.7 at.% silicon (Figure 7, Table 3).

(Insert Fig 10 near here)

The magnified GDOES profile for silicon disclosed a relatively high concentration the near surface region (Figure 4(d)). Phosphorus and silicon species were present throughout the remainder of the coating thickness, at the available resolution, with silicon increasing near to the metal/coating interface. The ratio of intensities of the phosphorus and oxygen signals was similar to the value for the coating formed in the individual electrolyte, while the corresponding ratio for silicon and oxygen was much reduced. The silicon peak near to the metal was not displaced below the depth of the main coating, contrary to findings for the phosphorus peak for the reverse sequence of electrolytes. Sodium was found at all depths in the coating. The time to sputter through the coating was increased to about 102 s, compared with 72 s for the previous experiment, correlating with the enhanced coating thickness determined in cross-sections. The SEM and GDOES data are consistent with relatively uniform growth of coating material in the second stage of anodizing, unlike the incomplete surface coverage achieved previously when anodizing lastly in the phosphate electrolyte.

4. Discussion

4.1 Composition and structure of coatings

The present findings indicate that the coatings formed on titanium by galvanostatic anodizing in silicate and phosphate electrolytes, either individually or sequentially, contain amorphous and crystalline material, with the latter including anatase and rutile. The remaining material is amorphous. No crystalline phases specific to silicon and phosphorus species were resolved. Thus, these species may be mainly solutes in the anatase and rutile phases or constituents of the amorphous phase. GDOES identified relatively uniform distributions of phosphorus and silicon species throughout the coating depth following anodizing in the individual electrolytes. The amounts of phosphorus and silicon in the local regions of phosphorus-rich and silicon-rich materials following sequential anodizing are about 5 – 8 and 10 – 20 at.% respectively. The corresponding atomic ratios with respect to titanium are on average 0.22 and 0.67, with maximum values of 0.31 and 1.07. Silicon and phosphorus species incorporated into amorphous anodic titania below the sparking voltage from silicate and phosphate electrolytes are respectively immobile and inward migrating, in the former case probably due to their presence as units of SiO_2 while in the latter case probably due to the presence of PO_4^{3-} ions [16]. Under the more extreme current densities and temperatures encountered at breakdown sites, transformation to other species may take place. In addition to formation of coating material by anodic oxidation processes, material may also develop through plasma-chemical reactions in the breakdown channel, involving substrate and electrolyte components. The present coating materials account typically for about 20-30% of the charge passed in the external circuit during anodizing of the titanium under sparking conditions. The significant contribution to the reduced efficiency of coating growth probably comes from the extensive gas generation, including oxygen, during anodizing.

Examination, by TEM, of the coating formed sequentially in silicate then phosphate electrolytes revealed amorphous and crystalline regions of oxide near the metal. During anodizing near 293 K in the absence of sparks, amorphous titania forms by migration of Ti^{4+} ions outward and O^{2-} ions inwards, with a transport number of about 0.35 for the cations [17]. The migration process involves movements of ions by atomic distances, without short-circuit transport. Growth of crystalline anodic titanium oxide may be associated with increased anion transport by a largely short-circuit mechanism, according to the evidence of other oxides [18]. Ionic transport in the coating material formed under sparking is likely to be affected by high current densities and temperatures produced by the localization of the current at the breakdown sites, as well as the modification of the oxide by incorporation of phosphorus and silicon species. Oxygen is also generated at sites of crystallinity in anodic titania, the gas initially being retained within the oxide prior to its release as the film ruptures [19]. Incorporation of foreign species into amorphous titania from either the electrolyte or from the metal can inhibit the transformation of amorphous material to a crystalline form and hence, suppress generation of oxygen [16]. Silicon species appear to be more effective than phosphorus species in stabilizing amorphous phases of the present coatings. In addition to generation associated with crystalline oxide, oxygen, together with peroxide, can also be formed in the discharge channel, possibly by plasma-chemical reactions or dissociation of water [20]. Further, altered near-surface pH through generation of hydrogen ions during growth of anodic oxide can lead to changes in the chemistry of the solution and deposition of gels [21]. Such altered surface chemistries may facilitate incorporation of electrolyte species into the coating material by reaction with either ionic or molecular entities in the solution or deposits

4.2 Sequential anodizing in silicate then phosphate electrolytes

The galvanostatic anodizing of titanium in silicate electrolyte under sparking conditions, followed by further anodizing with sparking in phosphate electrolyte provided tracer silicon and phosphorus species in the coating that assist understanding of the coating growth. Notably, the selected re-anodizing conditions allowed partial coverage of the macroscopic surface of the specimen by coating material formed in phosphate electrolyte, reflecting coating growth by localized processes at breakdown events with associated sparks. Evidently, the individual breakdown events result in incorporation of phosphorus species into most regions of the coating thickness, as averaged by GDOES over a large area, but with increased amounts at the coating surface and at the metal/coating interface. At the former location, phosphorus-containing coating material surrounds the pores formed due to breakdown in the phosphate electrolyte. The breakdown in phosphate electrolyte leaves mainly isolated tracks of transformed surface morphology of width about 20 - 100 μm and length about 1 mm, which also branch, within the remaining coating material, with characteristic morphology of the silicate electrolyte.

At the base of the coating, phosphorus-containing coating material is formed locally accompanied by increased consumption of the metal. Thus, at such locations, the thickness of the coating is enhanced relative to adjacent coating material formed in silicate electrolyte. The latter material is essentially phosphorus-free since breakdown in phosphate electrolyte has not occurred in these regions. The material in the intervening parts of the coating, i.e. located between the phosphorus-rich surface and

inner layers, consists of regions of silicon-containing coating material, of phosphorus-containing coating material and of a mixed type. The last two materials are located near the breakdown sites produced in phosphate electrolyte. Notably, EDX analyses at breakdown sites in the phosphate electrolyte indicated reduced levels of silicon, suggesting that the breakdown event leads to local loss of original silicon-containing material.

Clearly, the breakdown events lead to new coating material being localized near the coating surface, within the coating and near the metal, with GDOES indicating respective volume proportions of roughly 30%, 20% and 50% from the integrated intensities of the phosphorus signal at the three locations, assuming Gaussian-type tails on signals in the three regions. The proportions assume that the coating material formed in phosphate electrolyte is similar at all locations, which is in reasonable agreement with indications of GDOES for anodizing in the single electrolytes. The amount attributed to the surface region is probably an upper limit, since a reduced value of about 10% may be estimated for the surface region if data only for the first 10 s of sputtering are considered.

4.3 Sequential anodizing in phosphate then silicate electrolytes

For the selected conditions of the reverse sequence of anodizing, sufficient time was available for coating growth in silicate electrolyte over the macroscopic surface, which largely obscured the previous morphology of the coating developed in the phosphate electrolyte. However, GDOES indicated the location of new material at the coating surface, within the coating bulk and near the metal, consistent with a

behaviour broadly similar to that in phosphate electrolyte. However, the relative intensities of the integrated silicon signal for these regions indicate respective proportions of roughly 35, 20 and 45% of new coating material at these sites. As previously, the surface level is possibly an upper limit.

4.4 Mechanism of coating growth

The phenomenological evidence here indicates that breakdown allows access of electrolyte species to the inner part of the coating. The initiation of a breakdown event has not been directly examined here, but may be associated with cracks and gas bubbles in the coating or electron injection into the coating [22]. The current is subsequently focused at the breakdown site generating high temperatures and rapid growth of new coating material near the base of the coating, where the field is increased due to the penetration of the outer coating material by the electrolyte. High pressure is also likely in this region due to the generation of oxygen and steam, and to the volume changes resulting from conversion of metal into oxide, the Pilling-Bedworth ratio of TiO_2/Ti being about 1.76 for formation of anatase. Under a high electric field, amorphous anodic films can accommodate expansion of gas bubbles and non-uniform current flows near room temperature, exhibiting a plastic-like behaviour [23]. In association with softening at high temperature, coating material may be extruded along a breakdown channel, kept open by evolution of gas and electrolyte evaporation, possibly with spreading outward over the surface under the expansion of high-pressure gas bubbles.

The ready access of the electrolyte components to the inner parts of the coating at breakdown sites probably explains also evident the presence of sodium at practically all depths of the coating. In anodizing below the breakdown voltage, sodium ions are not incorporated into anodic films in significant amounts. Further, if incorporated by ion implantation, alkali metal ions migrate outward under the prevailing electric field [24]. However, in the present coatings, electrolyte ingress follows breakdown of the coating, which provides short-circuit paths from the coating surface to near the metal. The correlation of peaks for sodium and phosphorus in GDOES data when anodizing firstly in silicate and then in phosphate electrolytes suggests the simultaneous entry of the two species. The sodium may subsequently migrate outward following incorporation into coating material or be trapped in voids and interstices and regions of material under low electric field.

The initial breakdown of the coating allows electrolyte ingress, growth of new coating material near the metal, resulting in local thickening of the coating, and recession of the metal/coating interface. The breakdown process is possibly halted by the increased thickness of oxide near the metal, which thickens the barrier layer and reduces the electric field in the outer part of the coating, and by the start of other breakdown events, which transfers current to the new sites of reduced resistance. The new sites may be initiated by adjacent breakdown events and the associated stresses and coating defects, leading to the observed tracks on coatings formed firstly in silicate and secondly phosphate electrolyte. In addition, coating sites that have not undergone breakdown for some time will be favoured increasingly, since the coating is thinner and the electric field will be greater than at other places.

Conclusions

1. Coatings formed under sparking conditions on titanium in the selected alkaline phosphate and silicate electrolytes consist of anatase, rutile and amorphous material, with incorporation of relatively uniform concentrations of phosphorus and silicon species throughout the coating thickness.

2. During anodizing under sparking of titanium in alkaline phosphate electrolyte, following previous coating growth in alkaline silicate electrolyte, new coating material, identified by the presence of phosphorus, is located mainly near the metal, with additional new material also found within the coating and at the coating surface. About 10 – 30% of the new material is located near to the coating surface and about 40 – 60% near to the metal, with similar findings for the reverse sequence of electrolytes.

3. Coating growth occurs mainly as discrete local increases in coating thickness at sites of sparking. Thus, in the initial stages of re-anodizing, the new coating material is located at the sparking sites, while elsewhere the coating is unchanged until breakdown spreads to these regions.

Acknowledgements

The authors are grateful to the Engineering and Physical Sciences Research Council (UK) for support of this work.

References

[1] A.L. Yerokhin, X. Nie, A. Leyland, A. Matthews, S.J. Dowey, Surf. Coatings Technol. **122** 73 (1999).

[2] W. Krysmann, P. Kurze, K.-H. Dittrich, H.G. Schneider, Cryst. Res. Technol. **19** 973 (1984).

[3] P. Kurze, W. Krysmann, H.G. Schnider, Cryst. Res. Technol. **21** 1603 (1986).

[4] L.A. Snezhko, L. S. Tikhaya; Yu.E. Udovenko, V.I. Chernenko, Zashchita Metallov. **27** 425 (1991).

[5] G.P. Wirtz, S.D. Brown, W.M. Kriven, Mater. Manufacturing Processes **6** 87 (1991).

[6] V.I. Belevantzev, O.P. Terleeva, G.A. Markov, E.K. Shulepko, A.I. Slonova, V.V. Utkin, Protection of Metals **34** 416 (1998).

[7] S.V. Gnedenkov, O.A. Khrisanfova, A.G. Zavidnaya, S.L. Sinebrukhov, A.N. Kovryanov, T.M. Scorobogatova, P.S. Gordienko, Surf. Coat. Technol. **123** 24 (2000).

[8] V.S. Rudnev, T.P. Yarovaya, D.L. Boguta, L.M. Tyrina, P.M. Nedozorov, P.S. Gordienko, J. Electroanal. Chem. **497** 150 (2001).

[9] O.A. Khrisanfova, L.M. Volkova, S.V. Gnedenkov, T.A. Kajdalova. P.S. Gordienko, Z. Neorgan. Khim. **40** 558 (1995).

[10] A.L. Yerokhin, V.V. Lyubimov, R.V. Ashitkov, Ceram. Internat. **24** 1 (1998).

[11] A.L.Yerokhin, A. Leyland, A. Matthews, Appl. Surf. Sci. **200** 172 (2002).

[12] V.S. Rudnev, T.P. Yarovaya, V.V. Konshin, E.S. Panin, A.S. Rudnev, P.S. Gordienko, Russ. J. Electrochem. **32** 893 (1996).

[13] V.S. Rudnev, I.V. Lukiyanchuk, D.L. Boguta, V.V. Kon'shin, A.S. Rudnev, P.S. Gordienko, Protection of Metals, **38** 191 (2002).

[14] V.S. Rudnev, P.S. Gordienko, T.P. Yarovaya, E.S. Panin, G.I. Konshina, N.V. Chekatun, Electrokhimija **30** 914 (1994).

[15] F. Monfort, A. Berkani, E. Matykina, P. Skeldon, G.E. Thompson, H. Habazaki, K. Shimizu, J. Electrochem. Soc. **152** C382 (2005).

[16] H. Habazaki, K. Shimizu, S. Nagata, P. Skeldon, G.E. Thompson, G.C. Wood, Corros. Sci. **44** 1047 (2002).

[17] N. Khalil, J.S.L. Leach, Electrochim. Acta **31** 1279 (1986).

[18] J.P.S. Pringle, Electrochim. Acta **25** 1420 (1980).

[19] H. Habazaki, M. Uozumi, H. Konno, K. Shimizu, P. Skeldon, G. E. Thompson, Corros. Sci. **45** 2063 (2003).

[20] L.O Snizhko, A.L. Yerokhin, A. Pilkington, N.L. Gurevina, D.O. Misnyankin, A. Leyland, A. Matthews, Electrochim. Acta **14** 2085 (2004).

[21] J.R. Morlidge, P. Skeldon, G.E. Thompson, H. Habazaki, K. Shimizu, G.C. Wood, Electrochim. Acta **44** 2423 (1999).

[22] F. Di Quarto, S. Piazza, C. Sunseri, J. Electroanal. Chem. **248** 99 (1988).

[23] X. Zhou, G.E. Thompson, M.A.Paez, P. Skeldon, H. Habazaki, K. Shimizu, G.C. Wood, J. Electrochem. Soc. **147** 1747 (2000).

[24] F. Brown, W.D. Mackintosh, J. Electrochem. Soc **120** 1096 (1973).

Figure Captions

Figure 1(a). Voltage-time responses for titanium anodized at 2 A/dm^2 and 293 K: (a) in individual silicate and phosphate electrolytes for 900 s; (b) in silicate electrolyte to 360 V for 1200 s, then in phosphate electrolyte to 435 V for 1500 s; (c) in phosphate electrolyte to 435 V for 900 s, then in silicate electrolyte to 380 V for 600 s.

Figure 2. Dependence of coating thickness on charge density for titanium anodized at 2 A/dm^2 in silicate and phosphate electrolytes at 293 K

Figure 3. Scanning electron micrographs of titanium anodized at 2 A/dm^2 and 293 K: a) in silicate electrolyte to 360 V for 900 s; b) in phosphate electrolyte to 435 V for 900 s.

Figure 4. GDOES depth profiles of titanium anodized at 2 A/dm^2 and 293 K: a) in phosphate electrolyte to 435 V for 900 s; b) in silicate electrolyte to 360 V for 900 s; c) in silicate electrolyte to 360 V for 1200 s followed by anodizing in phosphate electrolyte to 435 V for 1200 s; d) in phosphate electrolyte to 435 V for 900 s, followed by anodizing in silicate electrolyte to 380 V for 600 s. The line labeled Fi characterizes change of the sputtering rate.

Figure 5. X-ray diffraction data of titanium anodized at 2 A/dm^2 and 293 K: 1) in phosphate electrolyte to 435 V for 900 s; 2) in silicate electrolyte to 360 V for 1200 s followed by anodizing in phosphate electrolyte to 435 V for 1500 s; 3) in silicate electrolyte to 360 V for 1200 s.

Figure 6. Scanning electron micrographs of titanium anodized at 2 A/dm^2 in silicate electrolyte to 360 V for 1200 s followed by anodizing in phosphate electrolyte to 435 V for 1500 s: a) plan view; b) 75^o tilt; c) ultramicrotomed cross-section.

Figure 7. Results of EDX analyses of the coatings at the points specified in Figs 6 and 8.

Figure 8. Scanning electron micrograph titanium after sputtering of the coating produced by anodizing at 2 A/dm^2 and 293 K to 360 V at in silicate electrolyte for 1200 s followed by anodizing to 435 V in phosphate electrolyte for 1200 s.

Figure 9. Transmission electron micrographs of titanium anodized at 2 A/dm^2 and 293 K to 360 V in silicate electrolyte for 1200 s followed by anodizing to 435 V in phosphate electrolyte for 1500 s. (a,b) – different sections.

Figure 10. Scanning electron micrograph of titanium anodized at 2 A/dm^2 and 293 K to 435 V in phosphate electrolyte to 435 V for 900 s followed by anodizing to 380 V in silicate electrolyte for 600 s.

Table 1. Thickness of coatings on titanium anodized at 2 A/dm^2 in silicate and phosphate electrolytes at 293 K.

Electrolyte	Charge density, kC/dm^2	Thickness, μm	Current efficiency, %
Silicate	1.2	1.4	44
	1.8	3.3	34
	2.4	4.3	33
	3.6	6.1	32
	4.8	7.6	30
	7.2	8.1	21
Phosphate	1.2	4.0	62
	2.4	5.8	45
	3.6	6.7	35
	4.8	7.4	29
	7.2	8.2	21

Table 2. Parameters of sequential anodizing of titanium at 2 A/dm^2 in silicate and phosphate electrolytes at 293 K.

Expt.	Electrolyte sequence	Sparking voltage, V	Forming voltage, V	Anodizing time, S	Charge density, kC/dm^2	Coating thickness, μm	Current efficiency, %	Charge density to restore sparking, kC/dm^2
1.	1st- Silicate	220	360	1200	2.4	4.3	33.4	
	2nd Phosphate	400	435	1500	3.0	5.6	6.2	2.6
2.	1st-Phosphate	290	435	900	1.8	5.1	52.8	
	2nd-Silicate	320	380	600	1.2	6.7	24.1	0.2

Table 3. Results of EDX analyses (at.%) of coatings. Si/P and P/Si are overall analyses of coatings formed sequentially in silicate then phosphate and phosphate then silicate respectively. Other analyses were made at points indicated in Figs 6 and 8.

	kV	Si/P	P/Si	P1	P2	P3	P4	Si1	Si2	Si3	Si-P
O	20	56.5	61.9	52.2	54.2	64.2	49.9	54.8	60.5	51.9	60.2
	10			70.3	71.6	71.5		57.8	70.7	70.4	
Si	20	6.7	5.7	0.7	<0.1	<0.2		23.2	11.2	6.5	2.0
	10			0.5	0.2	0.3		19.9	10.8	12.5	
P	20	4.5	2.3	8.4	2.7	7.8	2.8	0.3	0.2	0.4	6.6
	10			6.8	6.3	2.9		<0.1	5.0	0.1	
Ti	20	32.4	30.1	32.4	43.1	27.9	47.3	21.7	28.0	41.2	31.2
	10			22.2	21.9	25.3		22.3	13.6	17.1	

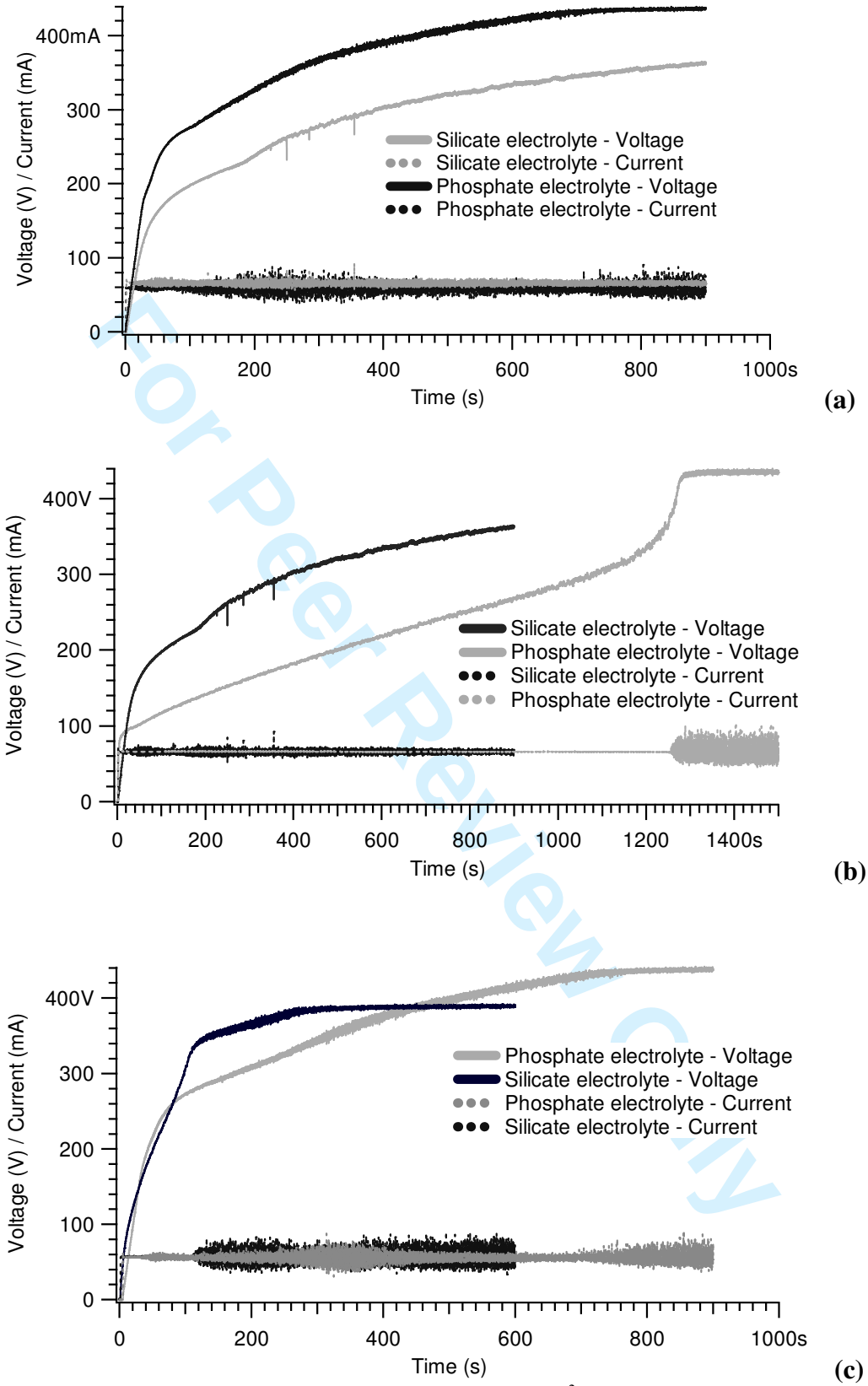

Figure 1. Voltage-time responses for titanium anodized at 2 A/dm^2 and 293 K (a) in individual silicate and phosphate electrolytes for 900 s; (b) in silicate electrolyte to 360 V for 1200 s, then in phosphate electrolyte to 435 V for 1500 s; (c) in phosphate electrolyte to 435 V for 900 s, then in silicate electrolyte to 380 V for 600 s.

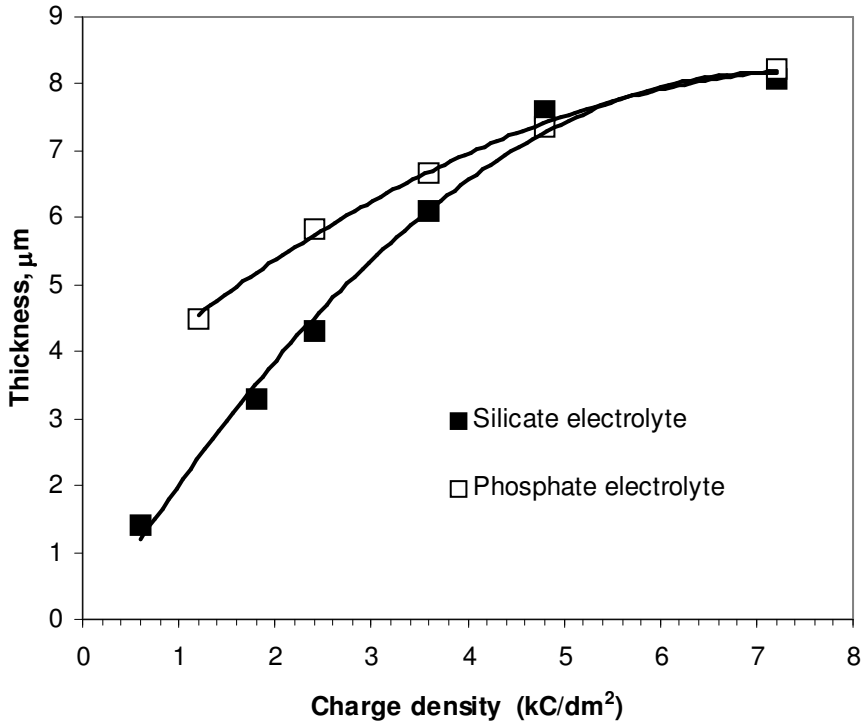

Figure 2. Dependence of coating thickness on charge density for titanium anodized at 2 A/dm^2 in silicate and phosphate electrolytes at 293 K

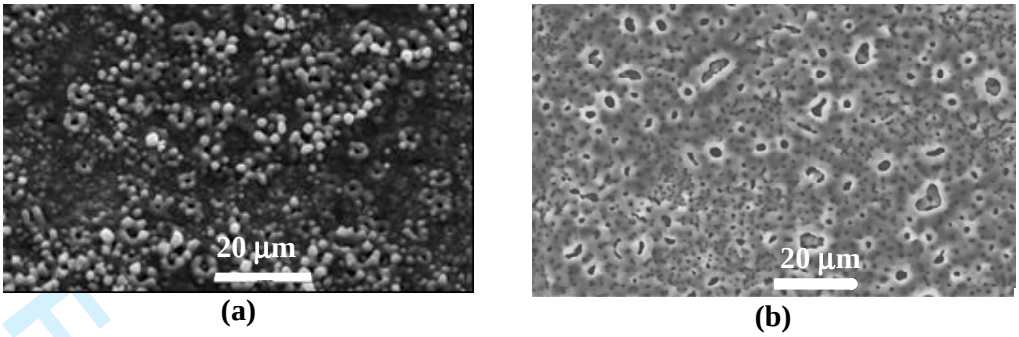

Figure 3. Scanning electron micrographs of titanium anodized at 2 A/dm^2 and 293 K: a) in silicate electrolyte to 360 V for 900 s; b) in phosphate electrolyte to 435 V for 900 s.

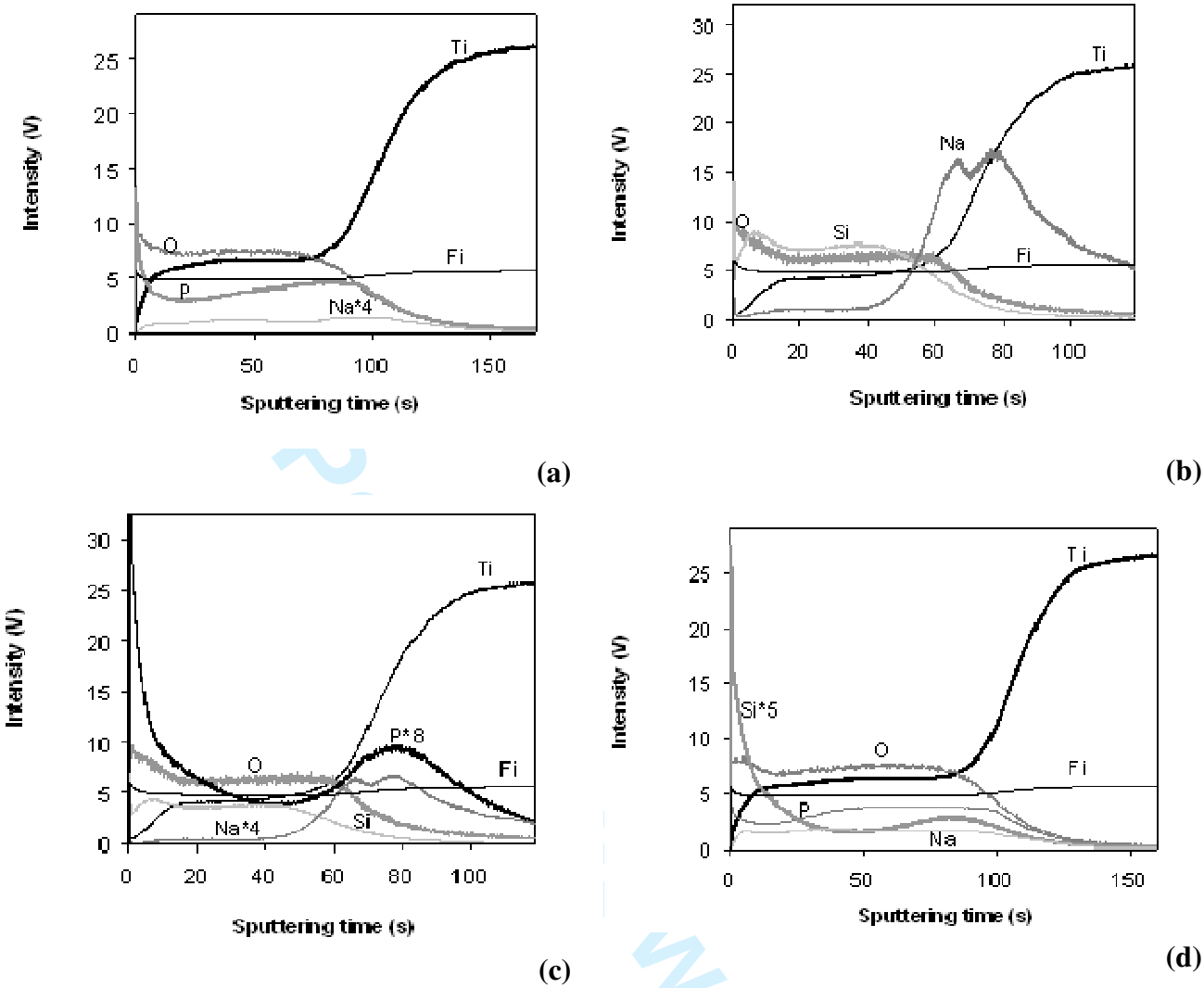

Figure 4. GDOES depth profiles of titanium anodized at 2 A/dm^2 and 293 K: a) in phosphate electrolyte to 435 V for 900 s; b) in silicate electrolyte to 360 V for 900 s; c) in silicate electrolyte to 360 V for 1200 s followed by anodizing in phosphate electrolyte to 435 V for 1200 s; d) in phosphate electrolyte to 435 V for 900 s, followed by anodizing in silicate electrolyte to 380 V for 600 s. The line labeled Fi characterizes change of the sputtering rate.

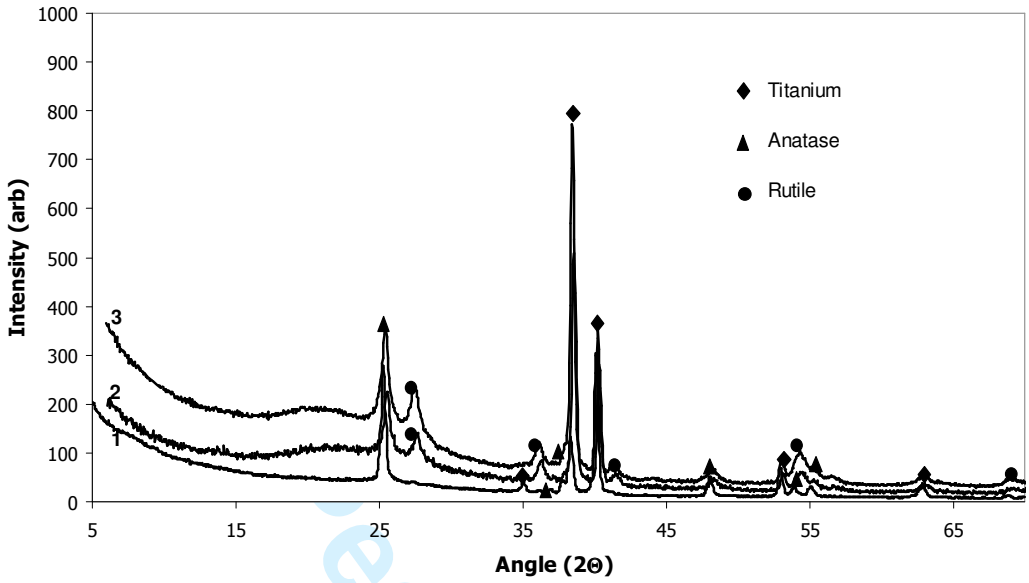

Figure 5. X-ray diffraction data of titanium anodized at 2 A/dm^2 and 293 K: 1) in phosphate electrolyte to 435 V for 900 s; 2) in silicate electrolyte to 360 V for 1200 s followed by anodizing in phosphate electrolyte to 435 V for 1500 s; 3) in silicate electrolyte to 360 V for 1200 s.

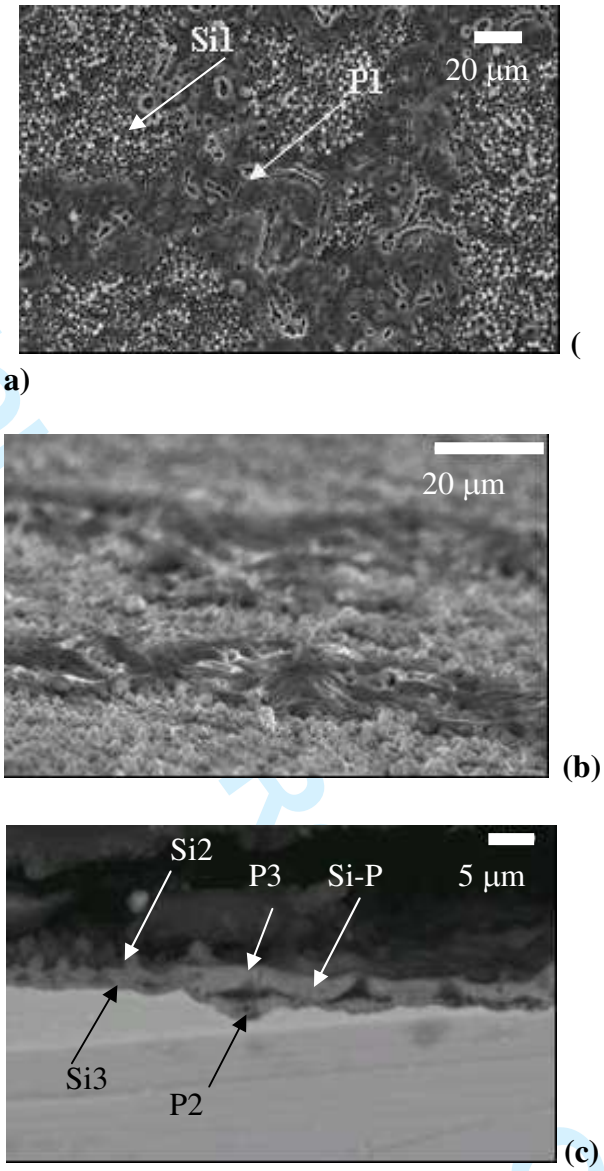

Figure 6. Scanning electron micrographs of titanium anodized at 2 A/dm^2 in silicate electrolyte to 360 V for 1200 s followed by anodizing in phosphate electrolyte to 435 V for 1500 s: a) plan view; b) 75^o tilt; c) ultramicrotomed cross-section.

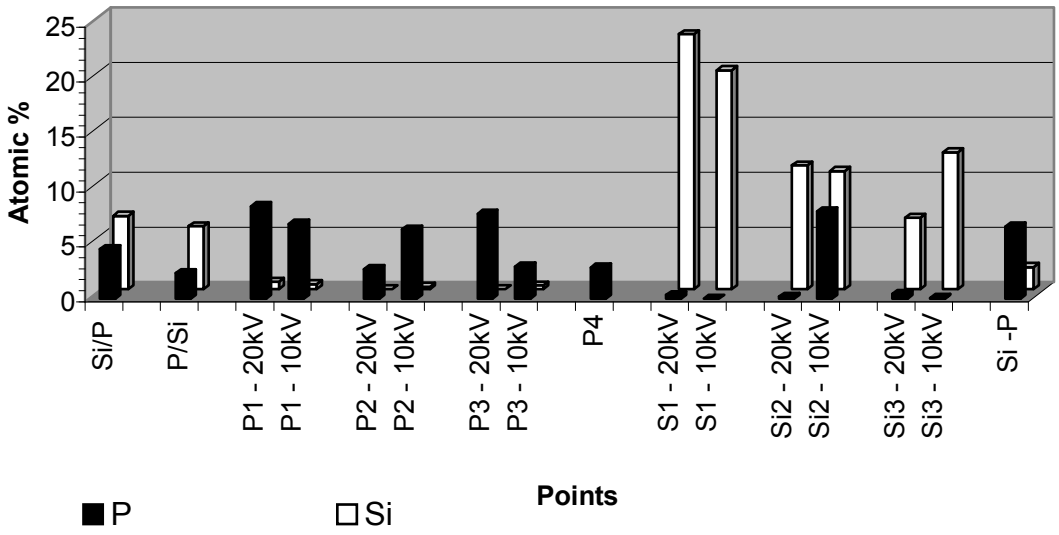

Figure 7. Results of EDX analysis of the coatings at the points specified in Figs 6 and 8.

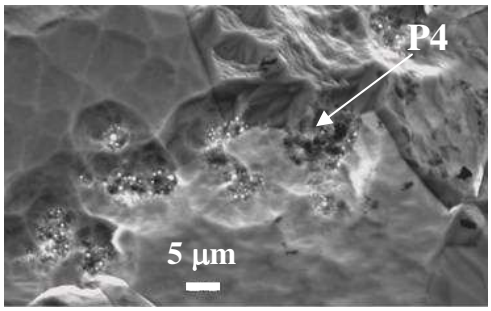

Figure 8. Scanning electron micrograph titanium after sputtering of the coating produced by anodizing at 2 A/dm^2 and 293 K to 360 V at in silicate electrolyte for 1200 s followed by anodizing to 435 V in phosphate electrolyte for 1200 s.

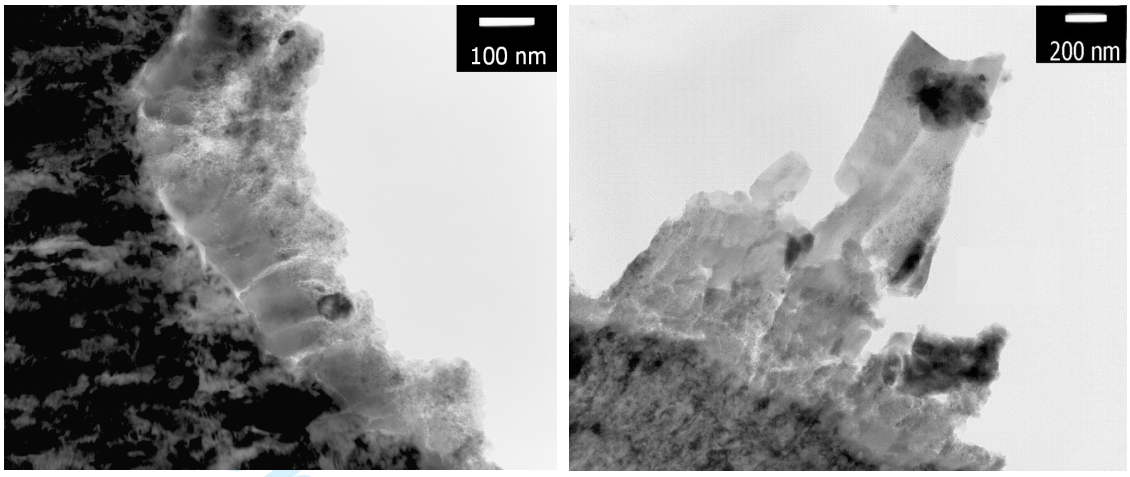

(a) **(b)**

Figure 9. Transmission electron micrographs of titanium anodized at 2 A/dm^2 and 293 K to 360 V in silicate electrolyte for 1200 s followed by anodizing to 435 V in phosphate electrolyte for 1500 s. (a, b) – different areas of the section.

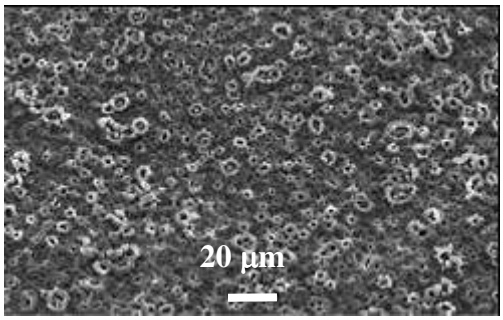

Figure 10. Scanning electron micrograph of titanium anodized at 2 A/dm^2 and 293 K to 435 V in phosphate electrolyte to 435 V for 900 s followed by anodizing to 380 V in silicate electrolyte for 600 s.